




Investigation of 2D Soot Distribution and Characteristic Soot Volume Fraction of Flames in the Confined Compartment with a Horizontal Opening

Wenbin Yao, Xiao Chen * and Shouxiang Lu*, State Key Laboratory of Fire Science, University of Science and Technology of China, Hefei 230026, China

Received: 24 May 2022/**Accepted:** 2 December 2022/**Published online:** 12 December 2022

Abstract. To comprehensively understand the effect of horizontal opening size on the soot evolution and transportation of flames in the confined compartment, 2D soot distribution and characteristic soot volume fraction of non-premixed propane flames were theoretically and experimentally investigated in the confined compartment (0.2 m × 0.2 m × 0.2 m) with different horizontal openings (0.03 m to 0.10 m) in this work. The oxygen concentration supplied by the horizontal opening was determined by the ratio of dimensionless opening size and dimensionless flame volume within a range of 14.5% to 20.7%. Results showed that the soot distribution of non-premixed propane flames in the confined compartment with a horizontal opening complied with the classical three-zone assumption. The maximum soot volume fraction, the characteristic length of the soot formation zone and the characteristic length of the soot oxidation zone were all positively related to the dimensionless flame volume and negatively correlated with the dimensionless opening size. There was a positive correlation between the ratio of two characteristic lengths and dimensionless flame volume, and the correlation was independent of the dimensionless opening size. Moreover, a linear correlation of characteristic soot volume fraction was proposed to predict the maximum soot volume fraction of non-premixed flames in the confined compartment with a horizontal opening.

Keywords: Confined compartment, Horizontal opening, Non-premixed flames, Laser-induced incandescence, Soot volume fraction

1. Introduction

Soot is the primary source of particulate pollution [1] and plays an important role in flame radiation heat transfer and fire spread [2]. The studies on soot formation and oxidation are helpful for us to understand the fire combustion mechanism

*Correspondence should be addressed to: Xiao Chen, E-mail: summercx@ustc.edu.cn Shouxiang Lu, E-mail: sxlu@ustc.edu.cn



and better control the generation and emission of particulate pollutants. In the past few decades, the soot evolution in various situations has been widely investigated through experiments [3–8] and numerical simulations [7–10]. Mahmoud et al. [3] observed log-normal conditional soot probability density functions across the full range of temperatures and found it was associated with a high degree of intermittency in soot turbulent fluctuations. The temperature and soot volume fraction measurements of a 2-m diameter pool fire reported by Sean et al. [4] agreed with the results obtained in Mahmoud [3] and provided valuable data for the development of soot radiation and emission models. Wei et al. [7] developed a global soot model for fires based on the previous studies [11–14], and made good agreements between the soot volume fraction predicted by numerical simulations and data measured by experiments. In a word, our understanding of soot formation and oxidation has evolved from a phenomenological explanation of laminar flames to an age of mathematical modeling for complex turbulent combustion and quantitative validation by experimental data [15].

Several works focused on the soot evolution in the compartment fire [16–19], and demonstrated that the incorporation of combustion, soot, and radiation models improved the fire parameter prediction in compartment fires with a vertical opening. Yuen et al. [19] compared the detailed soot formation for sooty and non-sooty flames in a door-ventilated ISO room using numerical and experimental methods, and he pointed out that the existing soot model might overestimate the soot mass fraction in compartment fires. Deepak et al. [20] measured the soot extinction coefficient of different liquid pool fires in the compartment and further estimated the soot yield. Gwon et al. [21] performed a mixture fraction analysis to study the characteristics of species production in compartment fires. They found that soot yield was a function of fuel types and local equivalence ratios in the upper layer.

It is surprising to note that little studies of soot evolution of flames in the confined compartments with horizontal openings have been reported. As one of the important research branch of the compartment fire, the confined compartment fire with horizontal openings was often a simplified model on the basis of the ship cabin, nuclear reactor and underground, etc. Previous works focused on the combustion characteristic parameters and fire behaviors of confined compartment fires with horizontal openings, such as burning rate [22, 23], temperature [24], product, flame shape [23], self-extinction [25], flame pulsation [26] and flame tilt [27]. Chen et al. [23] studied the burning characteristics of pool fires with different initial fuel depths inside a confined compartment with a horizontal opening and found that the burning rate presented the different trends with increasing fuel depth in the free burning atmosphere and the confined compartment. He et al. [25] investigated the self-extinction behavior of the pool fire in the compartment with a horizontal opening and established a model to predict the extinction time. As we all know that soot had a significant impact on the flow and thermal radiation characteristics, it is essential to investigate the flame structure as well as the production of smoke particulates to further characterize the flame behavior in the confined compartment with a horizontal opening. However, the effect of horizontal opening

size on the behavior of soot evolution and the characteristics of soot distribution in compartment fires has not been revealed.

In this work, a theoretical and experimental investigation of the 2D soot distribution of non-premixed propane flames in the confined compartment with a horizontal opening was conducted using the laser-induced incandescence (LII) technique. The 2D distributions of instantaneous soot volume fraction and average soot volume fraction were obtained. The statistical characteristics of maximum soot volume fraction were analyzed. The characteristic lengths of normalized soot distributions were proposed and correlated with the dimensionless opening sizes and dimensionless flame volumes. The relationship of characteristic soot volume fraction with the dimensionless opening sizes and dimensionless flame volumes was established, which could provide the theoretical guidance for the improvement of soot modeling of confined compartment fires with horizontal openings.

2. Theoretical Analysis for Soot Evolution of a Flame in the Confined Compartment

As shown in Fig. 1, whether in a free burning atmosphere or in a confined compartment, the soot evolution process could be divided into three zones: (1) the soot precursor zone, (2) the soot formation zone, and (3) the soot oxidation zone [28]. In zone I, the chemical reaction begins to generate the small aromatics and precursors of soot. The soot volume fraction increases very slowly. In zone II, incipient particles are formed by the precursors at a critical soot inception mixture fraction (ξ_c) in the mixture fraction space or equivalently at an initial height (L_c) in the geometric space. They grow continuously through surface growth, collision, and polymerization, which results in the graphitic aggregates and rapid increasing soot volume fraction. There exists a mixture fraction (ξ_m) or equivalently a height (L_m) that soot formation rate equals oxidation rate and the soot volume fraction reaches a maximum value. In zone III, the soot oxidation rate is higher than the formation rate. The oxidation products are formed and the soot volume fraction decreases to zero at the stoichiometric mixture fraction (ξ_{st}) or equivalently flame height (L_H) when no more fuel forms soot. The stoichiometric mixture fraction is defined as,

$$\xi_{st} = \left(1 + \frac{Y_{FT}M_{O_2}v_{O_2}}{Y_{O_2}M_Fv_F} \right)^{-1} \quad (1)$$

where Y_{FT} is the fuel mass fraction at the burner nozzle, Y_{O_2} is the oxygen mass fraction of air, M_F and M_{O_2} are the molecular weights of the fuel and oxygen, v_F and v_{O_2} are the stoichiometric coefficients of the fuel and oxygen in the chemical reaction. L_H , L_m , L_c in the geometric space can be associated with ξ_{st} , ξ_m , ξ_c in the mixture fraction space on the centerline of the flame [11]

$$L_m/L_H = \xi_{st}/\xi_m, L_c/L_H = \xi_{st}/\xi_c \quad (2)$$

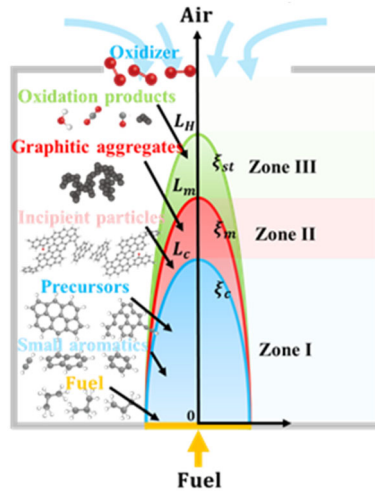


Figure 1. A sketch of soot evolution of a non-premixed flame and the opening air flow of a compartment fire with a horizontal opening. The flame is magnified in the figure to better illustrate the structure.

When the fuel is burned in the confined compartment as shown in Fig. 1, the horizontal opening is the only supplement of air. Therefore, the flame will be stretched to get enough oxygen. This phenomenon will be described in detail in the results. When the oxygen concentration falls below the critical oxygen concentration, the combustion could not be maintained and the flame is eventually extinguished.

The global soot model was initially proposed by Delichatsios [11] to describe the soot formation in an axisymmetric laminar non-premixed flame and then extended [12] by considering the temperature effect. In the soot formation zone, the modified volumetric soot formation rate could be expressed as

$$\dot{\omega}_{s,f}''' = A_f \rho^2 \left(Y_{F,1} \frac{\xi - \xi_{st}}{1 - \xi_{st}} \right) T^\gamma e^{-T_a/T}, \xi_m \leq \xi \leq \xi_c \quad (3)$$

where A_f is the pre-exponential factor of soot formation, ρ is the gas density, $Y_{F,1}$ is the fuel mass fraction at $\xi = 1$, γ is the temperature exponent and T_a is the activation temperature.

After neglecting the soot oxidation in the soot formation zone [11], the maximum value of soot volume fraction along the centerline can be estimated by integrating the Eq. (3) as:

$$f_{v,max} = \int_{L_c}^{L_m} \frac{\dot{\omega}_{s,f}'''}{\rho_s u_c} dz = \int_{L_c}^{L_m} \frac{A_f \rho^2 Y_{F,1}}{\alpha_u \rho_s \sqrt{g z}} \left(\frac{\xi - \xi_{st}}{1 - \xi_{st}} \right) T^\gamma e^{-T_a/T} dz \quad (4)$$

where u_c is the velocity along the centerline, ρ_s is the density of soot. Assuming $z/L_H = \xi_{st}/\xi$, the soot density and the temperature within the soot formation zone remain constant [29]. Equation (4) can be further transformed into the following form:

$$f_{v,max} = \frac{L_H A_f \rho^2 Y_{F,1} T^\gamma e^{-T_a/T}}{\alpha_u \rho_s \sqrt{g L_H}} \frac{\xi_{st}}{1 - \xi_{st}} fcn(\xi_c, \xi_m, \xi_{st}) \quad (5)$$

where $fcn(\xi_c, \xi_m, \xi_{st})$ is the function of ξ_c , ξ_m and ξ_{st} , and can be integrated as:

$$fcn(\xi_c, \xi_m, \xi_{st}) = 2 \left(\sqrt{\frac{\xi_{st}}{\xi_c}} + \sqrt{\frac{\xi_c}{\xi_{st}}} - \sqrt{\frac{\xi_{st}}{\xi_m}} - \sqrt{\frac{\xi_m}{\xi_{st}}} \right) \quad (6)$$

Overall, the maximum soot volume fraction of a non-premixed flame is associated with the flame height, the stoichiometric mixture fraction and $fcn(\xi_c, \xi_m, \xi_{st})$, which are affected by the oxygen concentration supplied by the limited horizontal opening and fuel property.

3. Experimental Approach

3.1. Flame Configurations

As shown in Fig. 2, the stable non-premixed flame was produced by a gas burner nozzle with an inner diameter (D) of 17.8 mm filled by perforated plates and ceramic beads. Propane was used as the fuel and the volume flow rate was controlled by a mass flow controller (MKS Instruments Inc. GE50A). The maximum volume flow rate of propane was 0.3 L/min with a maximum exit gas velocity of 0.02 m/s. The maximum Reynolds number ($Re = uD/\nu$, $\nu = 4.4 \text{ mm}^2/\text{s}$ for propane [30]) at the nozzle was 81. The inner dimension (d_0) of the confined compartment was 0.2 m, and the horizontal opening (d) ranged from 0.03 m to 0.1 m. The oxygen concentration near the flame base was measured by an electrochemical oxygen sensor (CiTiceL, AO₂) when the flame was stable enough. Detailed experimental conditions are shown in Table 1. 500 samples of instantaneous soot distribution were measured to study the statistics for each experimental condition. Each test was repeated at least four times and averaged to enhance the measurement accuracy, although the standard deviation of four tests was found to be less than 5.1%.

The oxygen consumed by the fuel combustion was closely related to the characteristic scale of confined compartment and flame characteristic scale. The characteristic scale of confined compartment, represented by the dimensionless opening size, was defined as the area ratio of the horizontal opening and the confined compartment,

$$\omega = d^2/d_0^2 \quad (7)$$

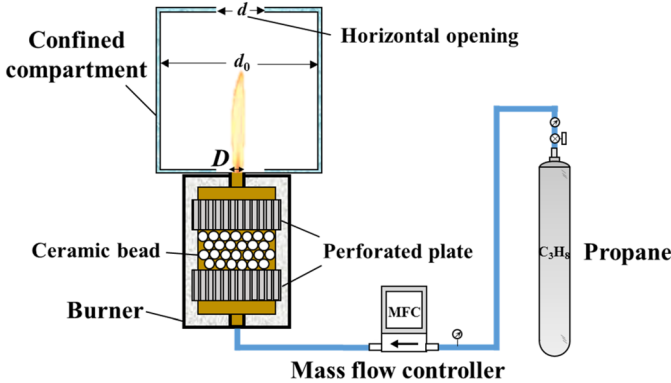


Figure 2. Gas burner configuration.

**Table 1
Summary of Experimental Conditions**

Test no	Volume flow rate (L/min)	Mass flow rate (mg/s)	Reynolds number	Opening size (m)	Oxygen concentration (%)
1–5	0.1–0.3	3.2–9.4	27–81	0.03	17.1–14.5
6–10				0.05	19.8–18.0
11–15				0.08	20.5–20.0
16–20				0.10	20.7–20.1

where d was the opening size and d_0 was the inner diameter of the confined compartment.

The flame characteristic scale, represented by the dimensionless flame volume, can be expressed as [31],

$$\Theta = V_f/d_0^3 = \left(\frac{\dot{Q}}{\rho_\infty c_p T_\infty \sqrt{g}} \right)^{6/5} / d_0^3 = \left(\frac{\rho_f \dot{V} \Delta h_c}{\rho_\infty c_p T_\infty \sqrt{g}} \right)^{6/5} / d_0^3 \quad (8)$$

where V_f was the flame volume and can be expressed as a function of the heat release rate or the volume flow rate for a given fuel type [32]. ρ_f and Δh_c were the gaseous density and the effective heat of combustion of fuel propane, $\rho_f = 1.8 \text{ kg/m}^3$ and $\Delta h_c = 43.70 \text{ MJ/kg}$. ρ_∞ , c_p and T_∞ were the density, the specific heat and the temperature of the air, $\rho_\infty = 1.2 \text{ kg/m}^3$, $c_p = 1.004 \text{ kJ/kg/K}$ and $T_\infty = 298 \text{ K}$.

Therefore, a dimensionless opening factor ω/Θ can be defined to connect the oxygen concentration X_{O_2} during the stabilization period of combustion with the horizontal opening size and volume flow rate of the fuel. As shown in Fig. 3, the dimensionless oxygen concentration first had rapid growth with the dimensionless opening factor and then slowly increased up to 1.

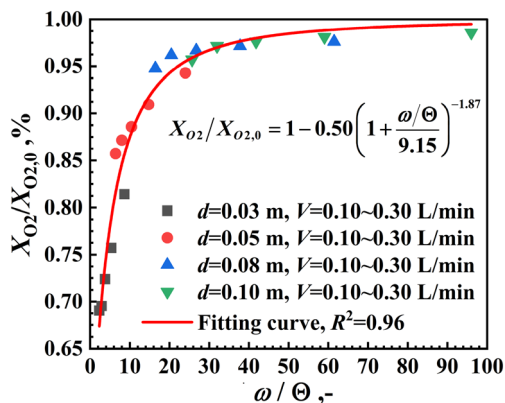


Figure 3. The oxygen concentration during the stabilization period of combustion varied with the dimensionless opening factor.

3.2. LII Experimental Setup

The laser-induced incandescence method is a visual and quantitative method of studying the 2D soot distribution of flames. It was also one of the most effective means to verify the theoretical model and numerical simulation of soot evolution in laminar and turbulent flames [33–36]. As shown in Fig. 4, a Nd: YAG laser (Beamtech SGR-30) with a frequency of 10 Hz and a pulse duration of 10 ns approximately was used in the LII experimental setup. The laser provided energy up to 1.2 J/pulse at 1064 nm. Therefore, the 532 nm laser with an energy output of 0.4 J/pulse was used in the present work. A laser sheet was created with an optical lens system, which consisted of a beam expander, a collimating lens ($f = 450$ mm), and a focus lens ($f = 600$ mm). The effective height of the laser sheet were 200 mm with a thickness of 0.5 mm. The total energy of laser sheet above the burner was about 180 mJ. Considering the energy variation across the laser sheet due to the Gaussian beam profiles, only 120 mm was actually used for LII measurements. The mean laser fluence in the zone of LII measurement was 0.23 J/cm^2 with a relative standard deviation of 8.4%, which agreed with the recommended value that the LII signal reached a plateau region at 532 nm and the laser irradiance caused minimal soot vaporization [37].

The incandescence signal was recorded at 10 frames per second with an intensified 1040×1392 pixel ICCD camera, which was equipped with a 50 mm zoom lens and a 410 nm optical filter. Two techniques were adopted in LII measurements to avoid the potential interference with other species [38]: (1) optical filter was placed in front of the camera to eliminate the laser diffusion effect [39]; (2) the collection of LII signals was delayed by 50 ns with an intensifier gate width of 50 ns to prevent the interferences of PAHs signal [38, 40].

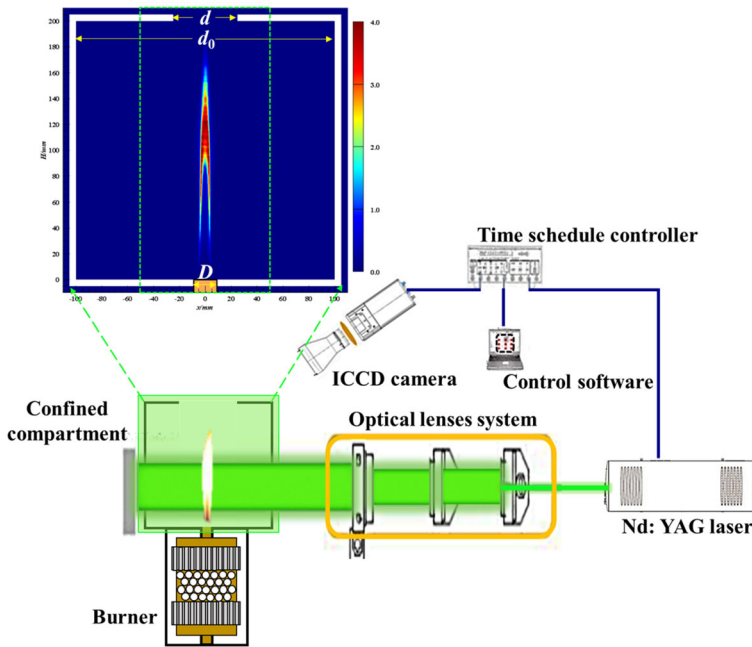


Figure 4. LII experimental setup.

3.3. Calibration and Process of LII Signal

LII signal was essentially a light intensity signal approximately proportional to the soot volume fraction [41]. The proportional coefficient of actual soot volume fraction and LII signal was closely related to experimental parameters. As shown in Fig. 5, two steps were taken to obtain the actual soot volume fraction of flames. The first step was to obtain the calibration coefficient of the actual soot volume fraction and LII signal. The calibration method of Francqueville [42] was used to determine the proportional coefficient:

$$\alpha = (\lambda_{LE} KL_{LEM}) / (k_e KL_{LII}) \quad (9)$$

where λ_{LE} was the LE laser wavelength, $\lambda_{LE} = 632.8 \text{ nm}$ and k_e was the dimensionless extinction coefficient, $k_e = 9.7$ for propane [43, 44], KL_{LII} was the integral value of LII signal within the LE optical path, KL_{LEM} was the cumulative value of optical-path soot volume fraction obtained by the laser extinction (LE) method and related to the attenuation of passing radiation by Lambert–Beer’s law [45],

$$KL_{LEM} = -\ln(I/I_0) \quad (10)$$

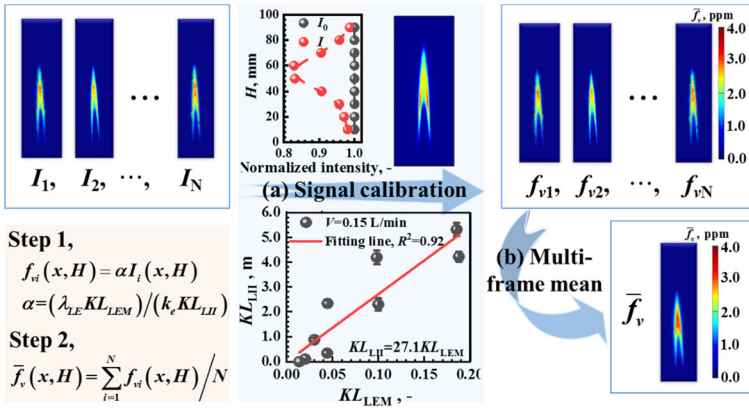


Figure 5. Calibration and process steps of LII signal.

where I_0 and I were the incident light and outgoing light of LE measurement, respectively, and were recorded by the digital oscilloscope and photoelectric receiver.

The distribution of soot volume fraction in the laminar diffusion flame was measured firstly on a Santoro gas burner using the LII system and LE method. In the calibration experiment, the propane flow was set at 0.15 L/min, and the co-flow air was set at 43 L/min to ensure that the co-flow air was adequate for combustion. Under these conditions, a stable laminar diffusion flame with a height of 90 mm could be obtained. The measured distribution of the LII signal and the normalized intensity of the LE light were shown in Fig. 5. The proportional coefficient of the actual soot volume fraction and LII signal, calculated by Eq. (9), can be expressed as

$$\alpha = 632.8 \times 10^{-9} / (9.7 \times 27.1) = 2.4 \times 10^{-9} \tag{11}$$

In addition, the second step was to process the multi-frame mean for each experimental condition. 500 LII images were taken when the flame was stable enough to reduce Gaussian noise.

4. Results and Discussions

4.1. 2D Distributions of Soot Volume Fraction

Typical 2D distribution of instantaneous soot volume fraction was shown in Fig. 6. For dimensionless opening size $\omega \leq 0.0625$, the 2D distribution of instantaneous soot volume fraction was stable during the stabilization period of combustion, and there was a slight oscillation for $\omega = 0.0225$, as shown in Fig. 6a and b. For $\omega = 0.25$, the 2D distribution of instantaneous soot volume fraction was unstable and flickering at a fixed frequency in the stabilization period, as shown in Fig. 6d. For $\omega = 0.16$, the 2D distribution of instantaneous soot volume fraction

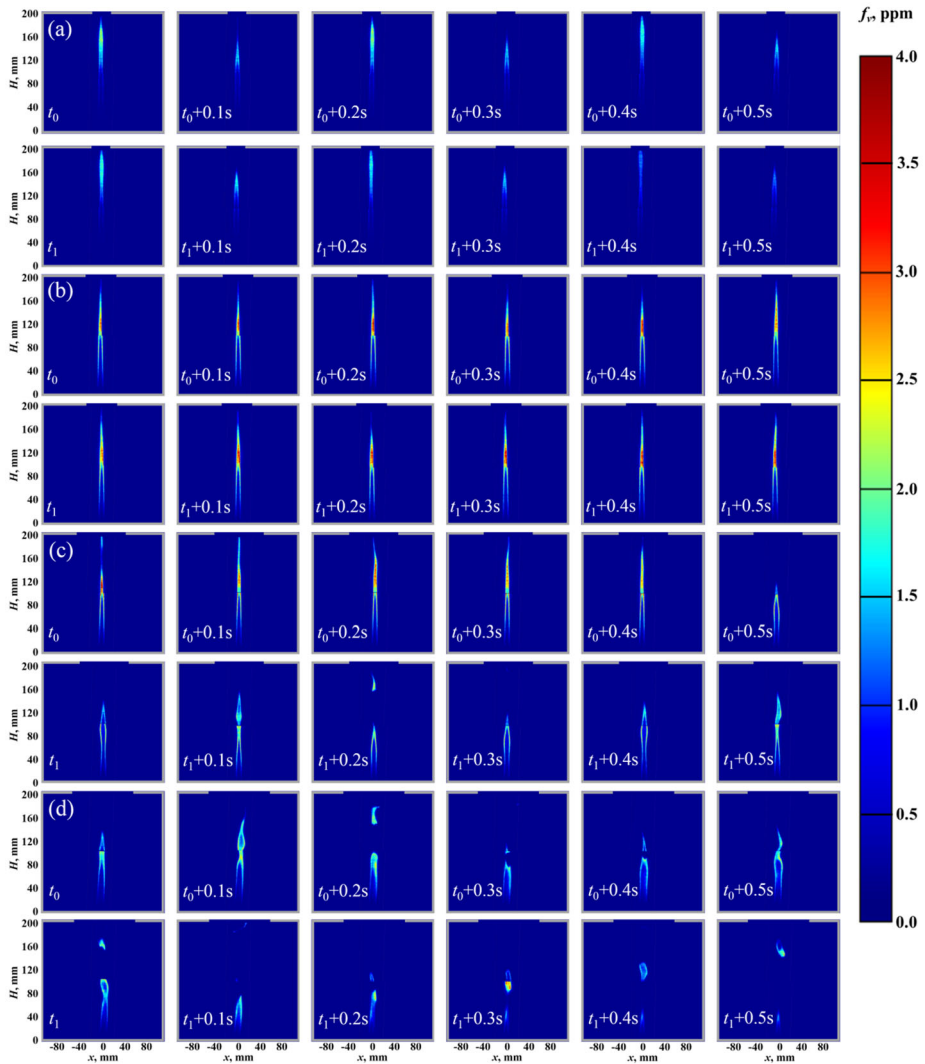


Figure 6. 2D distributions of the instantaneous soot volume fraction of propane flames ($\Theta = 0.0097$) in the confined compartment with different horizontal openings: a $\omega = 0.0225$, b $\omega = 0.0625$, c $\omega = 0.16$, d $\omega = 0.25$. t_0 and t_1 represent the time in the stabilization period of combustion.

was stable at some times and flickering at a fixed frequency at other times, as shown in Fig. 6c. The decrease of the proportion of flickering distribution of instantaneous soot volume fraction in the stabilization period may be affected by the change of flow pattern. Previous study [46] investigated the flow pattern induced by a fire in a ceiling vented enclosure, and found that there are three flow

patterns determined by the opening size and fire diameter: (a) unidirectional flow, transient and comparative stable; (b) bidirectional flow, transient and unstable; (c) compound flow, presented both a unidirectional flow and a bidirectional flow, transient, more complex and unstable than unidirectional flow and bidirectional flow. For dimensionless opening size $\omega \leq 0.0625$ in Fig. 6a and b, the stable instantaneous soot distribution was similar to the unidirectional flow pattern. The combustion product flowed out of the opening at some times and a small amount of air flowed into the opening to maintain the combustion at other times. For $\omega = 0.25$ in Fig. 6d, the unstable instantaneous soot distribution was similar to the bidirectional flow pattern. The combustion product and large amount of air could be well mixed so that the flame was unstable and flickering. For $\omega = 0.16$ in Fig. 6c, the soot distribution was stable at some time ($t_0 \sim t_0 + 0.5$ s), while unstable at other time ($t_1 \sim t_1 + 0.5$ s), which was similar to the compound flow pattern. The phenomena affected by unidirectional flow and bidirectional flow may appear alternately.

The 2D distributions of average soot volume fraction (SVF) were processed from 500 instantaneous images for each experimental condition. Figure 7 illustrated the 2D distributions of average soot volume fraction of propane flames for different dimensionless flame volumes and dimensionless opening sizes. The height of soot formation and oxidation zone, which could be represented by the height of 2D average SVF, increased with the decrease of dimensionless opening size for each dimensionless flame volume. The maximum value of 2D average SVF also increased with the decrease of dimensionless opening size, except for Fig. 7(1) and (5). For the cases with $0.0078 \leq \Theta \leq 0.0097$, the maximum value of 2D average SVF for $\omega = 0.0225$ was smaller than that for $\omega = 0.0625$ because self-extinguishing occurred for $\omega = 0.0225$. The maximum value of 2D average SVF was highest for $\Theta = 0.0078$ and $\omega = 0.0625$. As the dimensionless opening size decreased, the decreased proportion of flickering period of instantaneous soot volume fraction in the stabilization period of combustion was the reason for the increased average SVF.

4.2. Statistics on the Maximum Soot Volume Fraction

Two parameters were used to describe the statistical characteristics of maximum soot volume fraction. We defined $\overline{f_{v,max}}$ as the average value of maximum soot volume fraction, and $\overline{f_{v,max}}$ as the maximum value of the 2D distribution of average soot volume fraction. The different trends of calculated results of $\overline{f_{v,max}}$ and $\overline{f_{v,max}}$ varied with the volume flow rates were observed in Fig. 8a and b. $\overline{f_{v,max}}$ increased with the dimensionless flame volume and decreased with dimensionless opening size except for $\omega = 0.0225$ and $\Theta \geq 0.0060$. $\overline{f_{v,max}}$ first increased and then decreased with the increase of the dimensionless flame volume. $\overline{f_{v,max}}$ and $\overline{f_{v,max}}$ reached the maximum value at $\omega = 0.0225$ for $\Theta \leq 0.0042$, while reached the maximum value at $\omega = 0.0625$ for $\Theta \geq 0.0060$. The maximum soot volume fraction $\overline{f_{v,max}}$ is simultaneously affected by the soot formation rate and oxidation rate. For general situation, the increase of dimensionless flame volume increased

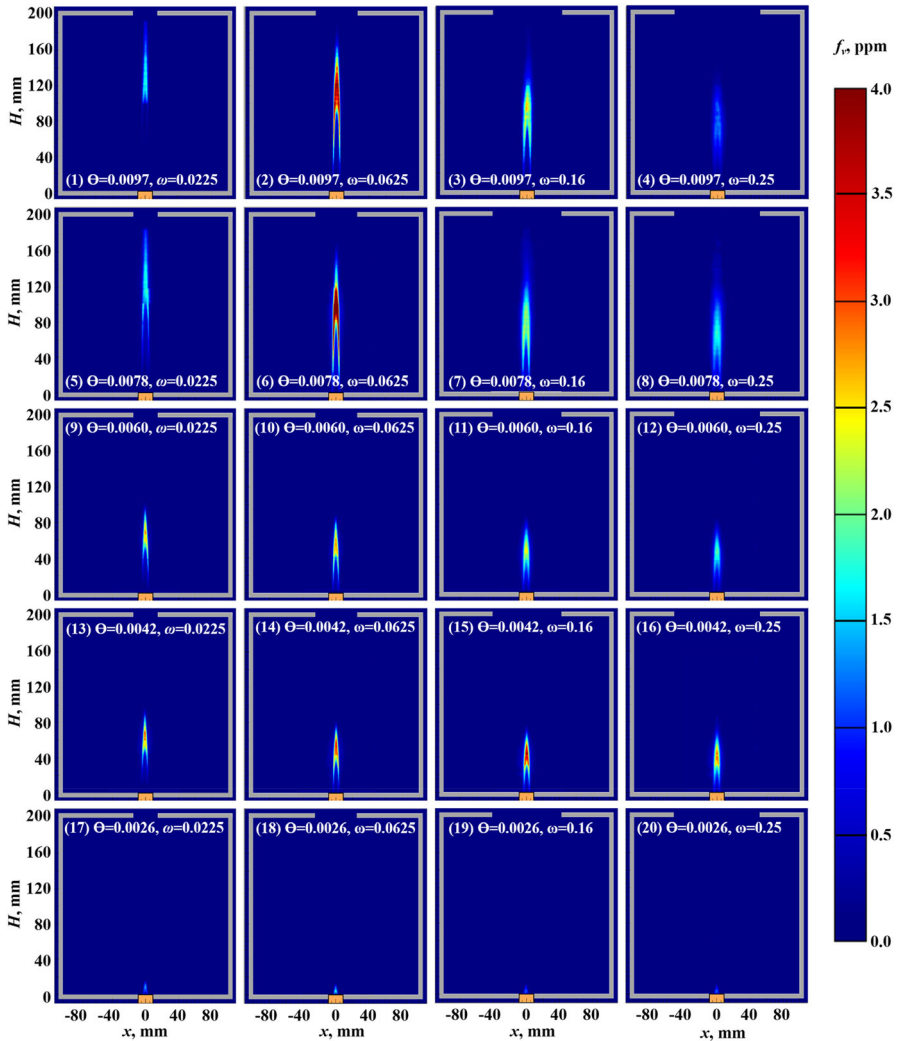


Figure 7. 2D distributions of the average soot volume fraction in the confined compartment with horizontal openings for different dimensionless opening sizes and dimensionless flame volumes.

the concentration of reactants involved in the soot formation reaction per unit compartment volume, and further increased the soot volume fraction; and the decrease of dimensionless opening size decreased the oxygen concentration, as well as the soot oxidation rate, and further increased the soot volume fraction. However, the increase of dimensionless flame volume increased the consumed oxygen, while the decrease of dimensionless opening size decreased the oxygen concentration in the compartment. Therefore, the flame with high dimensionless flame volume and small dimensionless opening size cannot maintain for a long time. The

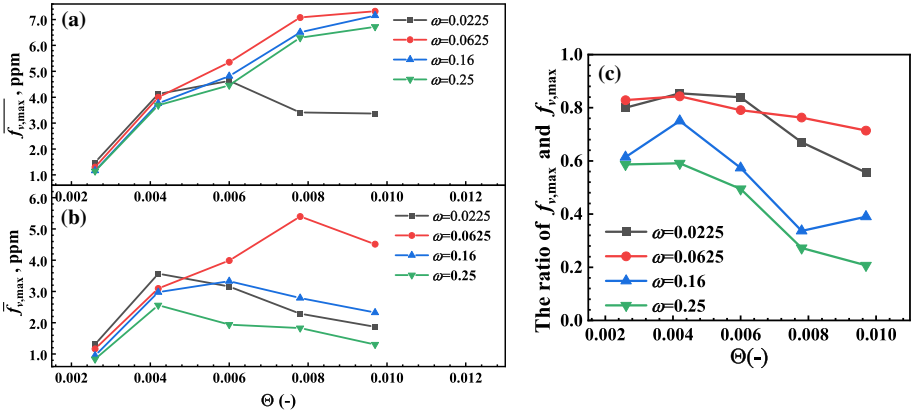


Figure 8. Three parameters **a** $\bar{f}_{v,max}$, **b** $\bar{f}_{v,max}$, **c** the ratio of $\bar{f}_{v,max}$ and $\bar{f}_{v,max}$ varied with the dimensionless flame volumes for different dimensionless opening size.

actual heat release may not be equal to the theoretical value, which is the possible reason for the fact that the soot volume fraction before extinguishment was lower than the expected result and reached the maximum value at $\omega = 0.0625$ for $\Theta \geq 0.0060$. The change of $\bar{f}_{v,max}$ was also affected by the soot intermittence, which can be estimated by the ratio of $\bar{f}_{v,max}$ and $\bar{f}_{v,max}$ as shown in Fig. 8c. The ratio of $\bar{f}_{v,max}$ and $\bar{f}_{v,max}$ decreased with the increase of dimensionless flame volume and dimensionless opening size to the minimum value of 0.2, which indicated that the flame was laminar and stable for the cases with low dimensionless flame volume or low dimensionless opening size, while the flame was turbulent and unstable for the cases with high dimensionless flame volume and high dimensionless opening size. For the turbulent flames, the soot existed at a certain position in the flame with a high degree of intermittence and the soot volume fraction was low for most of the time, which is the direct reason for the different trends of $\bar{f}_{v,max}$ and $\bar{f}_{v,max}$.

5. Characteristic Lengths L_m and L_H

Considering that the maximum value of the soot volume fraction in the flames was simultaneously affected by the soot formation rate and oxidation rate, the characteristic lengths (or characteristic mixture fractions) of the soot formation zone and soot oxidation zone may be the key to quantify the maximum soot volume fraction.

A normalization method was used to quantifying the characteristic lengths L_m and L_H . The normalized maximum of soot volume fraction was defined as:

$$\bar{f}_v^* = \bar{f}_{v,max}(H) / \bar{f}_{v,max} \in [0, 1] \tag{12}$$

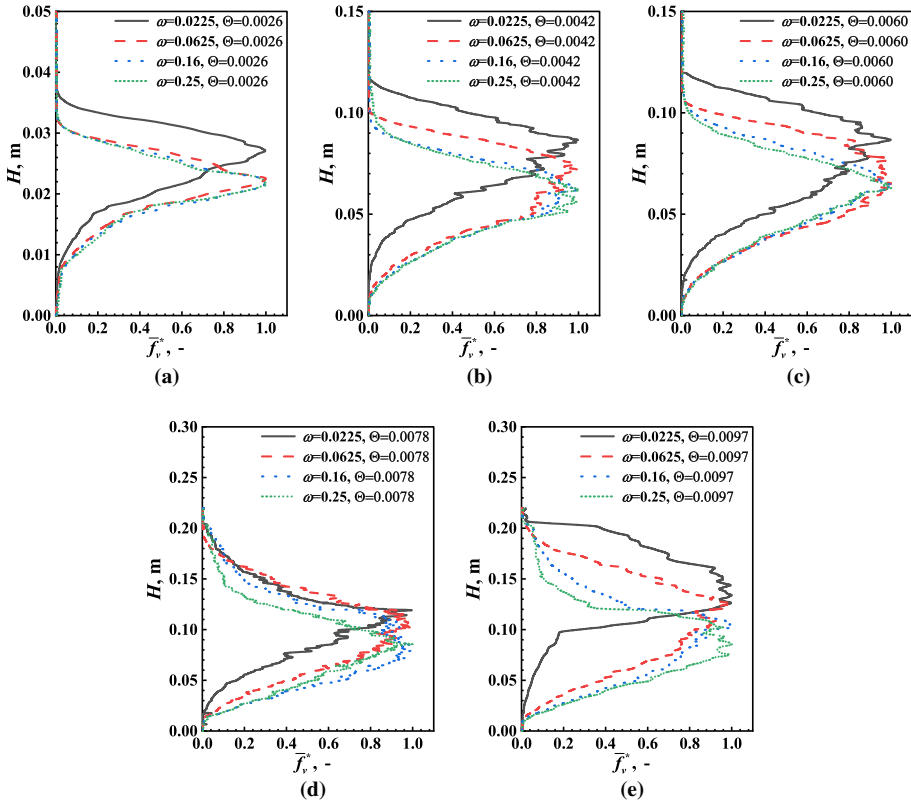


Figure 9. The profiles of \bar{f}_v of flames in the confined compartment with different horizontal openings for different dimensionless flame volumes: **a** $\Theta = 0.0026$, **b** $\Theta = 0.0042$, **c** $\Theta = 0.0060$; **d** $\Theta = 0.0078$; **e** $\Theta = 0.0097$.

where $\bar{f}_{v,max}(H)$ was the maximum value of the 2D distribution of the average soot volume fraction at the height H . Using the maximum profiles of different heights could avoid the underestimation of the maximum soot volume fraction along the centerline. Besides, the maximum profiles of soot represented the radiation ability of a flame at different heights.

The profiles of \bar{f}_v for various dimensionless flame volumes and dimensionless opening sizes were presented in Fig. 9. \bar{f}_v first increased and then decreased with the height. The height of $\bar{f}_v^* = 1$ increased with the dimensionless flame volume while decreasing with the dimensionless opening size. Actually, the dimensionless opening size affects the oxygen concentration of the confined compartment. The decrease of oxygen concentration increases the initial height of soot oxidation (the height of $\bar{f}_v^* = 1$).

\bar{f}_v and \bar{f}_v^* for the typical condition of $\Theta = 0.0097$ and $\omega = 0.0625$ were presented in Fig. 10. The height of $\bar{f}_v^* = 1$ was defined as the characteristic length L_m .

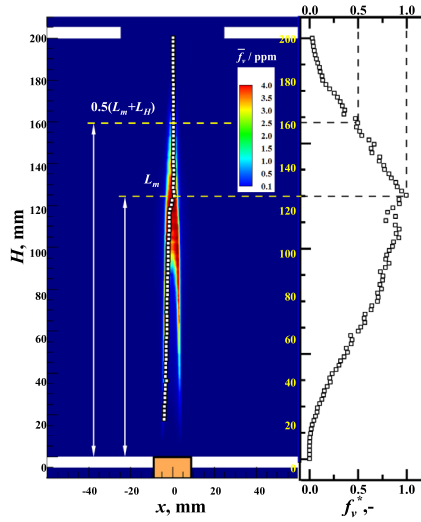


Figure 10. Characteristic lengths L_m and L_H in the 2D soot distribution for $\Theta = 0.0097$ and $\omega = 0.0625$.

After reaching the maximum value, the soot volume fraction decreased to zero due to soot oxidation. The height that the soot volume fraction decreased to zero was defined as the length of soot oxidation ending or equivalently the flame height L_H . However, the value of L_H was directly affected by the value of chosen threshold when processing the boundary of the soot zone. Thus, the height of $\bar{f}_v^* = 0.5$ was considered as $0.5(L_m + L_H)$ to avoid the impact of the threshold.

5.1. Correlation of Maximum Soot Volume Fraction with the Dimensionless Flame Volume and Dimensionless Opening Size

Based on the previous theoretical analysis and experimental results, a characteristic soot volume fraction was proposed to explore the effect of horizontal opening sizes on the value of maximum soot volume fraction in the following

$$\overline{f_{v,max}} / \left[fcn(\xi_c, \xi_m, \xi_{st}) L_H^{1/2} \right] \tag{13}$$

The function $fcn(\xi_c, \xi_m, \xi_{st})$ calculated by Eq. (6) was mainly controlled by the value of ξ_c/ξ_{st} (the ratio of L_H and L_c) and ξ_m/ξ_{st} (the ratio of L_H and L_m). The critical soot inception mixture fraction ξ_c was proportional to the stoichiometric mixture fraction ξ_{st} ($\xi_c/\xi_{st} = 2.5$) in previous studies [7, 47]. The relationship between ξ_m and ξ_{st} was shown in Fig. 11a. ξ_m/ξ_{st} was independent of the dimensionless opening size and increased from approximately 1.3 to 1.8 with an increase of dimensionless flame volume from 0.10 to 0.30 L/min. This indicated that the proportion of the height of the maximum soot volume fraction and the flame height decreased with the dimensionless flame volume. $\xi_m = 1.56\xi_{st}$ could be an

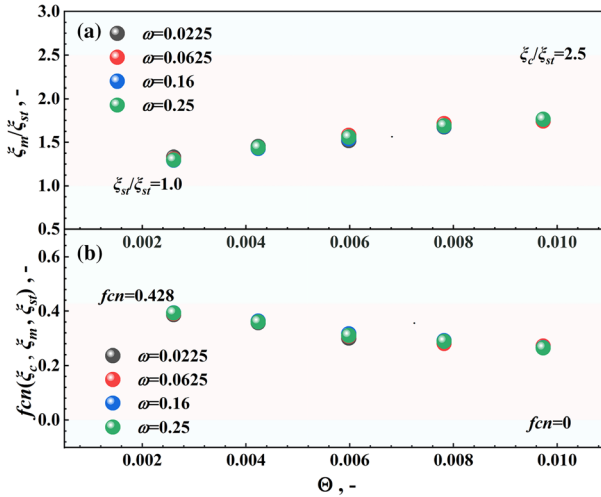


Figure 11. The values of a ξ_m/ξ_{st} and b $fcn(\xi_c, \xi_m, \xi_{st})$ varied with dimensionless flame volume for different dimensionless opening sizes.

estimated average value of the characteristic mixture fraction. $fcn(\xi_c, \xi_m, \xi_{st})$ decreased with the increase of the dimensionless flame volume as shown in Fig. 11b.

Figure 12 illustrates the characteristic soot volume fraction varied with the dimensionless flame volume for dimensionless opening sizes. The characteristic soot volume fraction presented a linear correlation with the increase of the reciprocal of dimensionless flame volume. The correlation could be shown in the following:

$$\overline{f_{v,max}} / [fcn(\xi_c, \xi_m, \xi_{st})L_H^{1/2}] = 154.00 - 0.32/\Theta \tag{14}$$

For $\omega = 0.0225$ and $\Theta \geq 0.0078$, self-extinguishing behavior happened and the flame could not maintain due to the lack of oxygen.

6. Conclusions

The present study theoretically and experimentally investigated the 2D soot distribution of non-premixed propane flames in the confined compartment with a horizontal opening using LII. The 2D soot distribution and characteristic soot volume fractions for different dimensionless opening sizes and dimensionless flame volumes were obtained. The major findings are:

- (1) The soot evolution process of a non-premixed flame in the confined compartment with a horizontal opening was examined to comply with the three zones

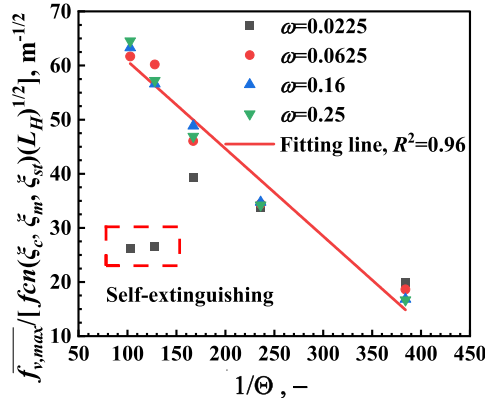


Figure 12. The characteristic soot volume fraction $f_{v,max} / [fcn(\xi_c, \xi_m, \xi_{st}) L_H^{1/2}]$ varied with the reciprocal of dimensionless flame volume for different dimensionless opening sizes.

by height: soot precursor zone, soot formation zone, and soot oxidation zone. The maximum soot volume fraction of a non-premixed flame in the confined compartment with a horizontal opening was theoretical analyzed and correlated with the flame height L_H , the stoichiometric mixture fraction ξ_{st} and $fcn(\xi_c, \xi_m, \xi_{st})$.

- (2) Time evolution of instantaneous soot volume fraction in the stabilization period of combustion was stable for dimensionless opening size $\omega \leq 0.0625$ and flickering for $\omega = 0.25$. As the dimensionless opening size decreased, the proportion of flickering period of instantaneous soot volume fraction descended. The maximum soot volume fraction increased with a fall of dimensionless opening size and increased with a rise of dimensionless flame volume. Under a condition of $\omega = 0.0225$ and $\Theta \geq 0.0078$, the flame could not maintain.
- (3) Characteristic lengths L_m and L_H were proposed in the analysis of the normalized soot distribution of the soot volume fraction. They were both positively proportional to the dimensionless flame volume and negatively related to the dimensionless opening size. There was a positive correlation between ξ_m/ξ_{st} (the ratio of L_H and L_m) and dimensionless flame volume and the correlation was independent of the dimensionless opening size. Characteristic soot volume fraction $f_{v,max} / [fcn(\xi_c, \xi_m, \xi_{st}) L_H^{1/2}]$ linearly correlated with the reciprocal of dimensionless flame volume, which was proposed to predict the maximum soot volume fraction of non-premixed flames in the confined compartment with a horizontal opening.

One of the limitations of the established model in this paper is that no comprehensive analysis of the joint impact of soot generation rate and oxidation rate on the peak volume fraction of soot has been made. It is assumed that the position of peak soot volume fraction L_m is the position where soot starts to oxidize. The position where the soot starts to oxidize is slightly lower than L_m . In addition, the method to accurately define the threshold of soot volume fraction measured by

LII is one of the urgent problems to be solved at present. The method used in this paper avoids the definition of the threshold, but the determination of L_H is affected by L_m to a certain extent.

In conclusion, although the established model in this paper simplified the soot evolution process in the confined compartment, the results show that the above simplification and assumption is acceptable within the scope of this study. Of course, further validation on a larger scale of confined compartment fire is needed for the expansion of the application of this model. Besides, it would be necessary to analyze the correlation between the maximum value and maximum position to improve the understanding of soot evolution and transportation of flames in the confined compartment with a horizontal opening.

Acknowledgements

This work was sponsored by National Natural Science Foundation of China (Grant No. 51704268), Fundamental Research Funds for the Central Universities (Nos. WK2320000044 and WK2320000048).

References

1. Seinfeld J, Pandis S (2008) Atmospheric chemistry and physics, 1997. New York
2. Cheung SC, Yuen RK, Yeoh G, Cheng GW (2004) Contribution of soot particles on global radiative heat transfer in a two-compartment fire. *Fire Saf J* 39:412–428
3. Mahmoud S, Nathan G, Medwell P, Dally B, Alwahabi Z (2015) Simultaneous planar measurements of temperature and soot volume fraction in a turbulent non-premixed jet flame. *Proc Combust Inst* 35:1931–1938
4. Kearney SP, Grasser TW (2017) Laser-diagnostic mapping of temperature and soot statistics in a 2-m diameter turbulent pool fire. *Combust Flame* 186:32–44
5. Jiang P, Zhou M, Wen D, Wang Y (2021) An experimental multiparameter investigation on the thermochemical structures of benchmark ethylene and propane counterflow diffusion flames and implications to their numerical modeling. *Combust Flame* 234:111622
6. Mannazhi M, Török S, Gao J, Bengtsson P-E (2021) Soot maturity studies in methane-air diffusion flames at elevated pressures using laser-induced incandescence. *Proc Combust Inst* 38:1217–1224
7. Wei Y, Zhang J, Nadjai A, Beji T, Delichatsios MA (2011) A global soot model developed for fires: validation in laminar flames and application in turbulent pool fires. *Fire Saf J* 46:371–387
8. Kruse S, Medwell P, Davidovic M, Sun Z, Ye J, Pitsch H, Dally BB (2021) The effect of fuel composition and Reynolds number on soot formation processes in turbulent non-premixed toluene jet flames. *Proc Combust Inst* 38:1395–1402
9. Liu F, Guo H, Smallwood GJ, Gülder ÖL (2003) Numerical modelling of soot formation and oxidation in laminar coflow non-smoking and smoking ethylene diffusion flames. *Combust Theor Model* 7:301

10. Hoerle CA, França FHR, Pagot PR, Pereira FM (2020) Effects of radiation modeling on non-premixed sooting flames simulations under oxyfuel conditions. *Combust Flame* 217:294–305
11. Delichatsios MA (1994) A phenomenological model for smoke-point and soot formation in laminar flames. *Combust Sci Technol* 100:283–298
12. Beji T, Zhang JP, Delichatsios M (2008) Determination of soot formation rate from laminar smoke point measurements. *Combust Sci Technol* 180:927–940
13. Lee KB, Thring MW, Beér J (1962) On the rate of combustion of soot in a laminar soot flame. *Combust Flame* 6:137–145
14. Leung KM, Lindstedt RP, Jones WP (1991) A simplified reaction mechanism for soot formation in nonpremixed flames. *Combust Flame* 87:289–305
15. Wang H (2011) Formation of nascent soot and other condensed-phase materials in flames. *Proc Combust Inst* 33:41–67
16. Moss J, Aksit I (2007) Modelling soot formation in a laminar diffusion flame burning a surrogate kerosene fuel. *Proc Combust Inst* 31:3139–3146
17. Yuen ACY (2014) On the prediction of combustion products and soot particles in compartment fires. University of New South Wales
18. Yuen A, Yeoh G, Timchenko V, Cheung S, Barber T (2016) Importance of detailed chemical kinetics on combustion and soot modelling of ventilated and under-ventilated fires in compartment. *Int J Heat Mass Transfer* 96:171–188
19. Yuen A, Yeoh G, Timchenko V, Chen T, Chan Q, Wang C, Li D (2017) Comparison of detailed soot formation models for sooty and non-sooty flames in an under-ventilated ISO room. *Int J Heat Mass Transfer* 115:717–729
20. Ko GH, Hamins A, Bundy M, Johnsson EL, Kim SC, Lenhert DB (2009) Mixture fraction analysis of combustion products in the upper layer of reduced-scale compartment fires. *Combust Flame* 156:467–476
21. Sahu D, Jain S, Gupta A, Kumar S (2019) Experimental studies on different liquid pool fires inside the compartment. *Fire Saf J* 109:102858
22. Yuan M, Chen B, Li C, Zhang J, Lu S (2013) Analysis of the combustion efficiencies and heat release rates of pool fires in ceiling vented compartments. *Procedia Eng* 62:275–282
23. Chen X, Lu S, Ding Z (2020) Initial fuel depth effect on the burning characteristics of thin-layer pool fire in a confined enclosure. *J Therm Anal Calorim* 139:1409–1418
24. Guo F, Wang C, Zhang J (2018) Spray fire induced gas temperature characteristics and correlations in a ceiling ventilated compartment. *Int J Therm Sci* 134:188–199
25. He Q, Ezekoye OA, Li C, Lu S (2015) Ventilation limited extinction of fires in ceiling vented compartments. *Int J Heat Mass Transfer* 91:570–583
26. Chen X, Lu S, Wang X, Liew KM, Li C, Zhang J (2016) Pulsation behavior of pool fires in a confined compartment with a horizontal opening. *Fire Technol* 52:515–531
27. Ding Z, Chen X, Lu S, Wang Y (2020) An investigation of flame tilt transition inside the compartment with horizontal opening in cross wind. *Proc Combust Inst* . <https://doi.org/10.1016/j.proci.2020.07.085>
28. Zhang P, Liu H-F, Chen B-L, Tang Q-L, Yao M-F (2015) Fluorescence spectra of polycyclic aromatic hydrocarbons and soot concentration in partially premixed flames of diesel surrogate containing oxygenated additives. *Wuli Huaxue Xuebao* 31:32–40
29. Lautenberger CW, Ris J, Dembsey NA, Barnett JR, Baum HR (2005) A simplified model for soot formation and oxidation in CFD simulation of non-premixed hydrocarbon flames. *Fire Saf J* 40:141–176
30. Lide DR (2006) CRC handbook of chemistry and physics, 86th edition. *J Am Chem Soc* 128:5585

31. Zhang J, Lu S, Li C, Yuan M, Yuen R (2013) On the self-extinction time of pool fire in closed compartments. *Procedia Eng* 62:266–274
32. Quintiere JG (2006) *Fundamentals of fire phenomena*. Wiley, New York
33. Xin Y, Gore JP (2005) Two-dimensional soot distributions in buoyant turbulent fires. *Proc Combust Inst* 30:719–726
34. Qamar N, Nathan G, Alwahabi Z, King K (2005) The effect of global mixing on soot volume fraction: measurements in simple jet, precessing jet, and bluff body flames. *Proc Combust Inst* 30:1493–1500
35. Qamar N, Alwahabi Z, Chan Q, Nathan G, Roekaerts D, King K (2009) Soot volume fraction in a piloted turbulent jet non-premixed flame of natural gas. *Combust Flame* 156:1339–1347
36. Köhler M, Geigle KP, Meier W, Crosland BM, Thomson KA, Smallwood GJ (2011) Sooting turbulent jet flame: characterization and quantitative soot measurements. *Appl Phys B* 104:409–425
37. Quay B, Lee T-W, Ni T, Santoro R (1994) Spatially resolved measurements of soot volume fraction using laser-induced incandescence. *Combust Flame* 97:384–392
38. Schulz C, Kock BF, Hofmann M, Michelsen H, Will S, Bougie B, Suntz R, Smallwood G (2006) Laser-induced incandescence: recent trends and current questions. *Appl Phys B* 83:333–354
39. Moreau CS, Therssen E, Mercier X, Pauwels J, Desgroux P (2004) Two-color laser-induced incandescence and cavity ring-down spectroscopy for sensitive and quantitative imaging of soot and PAHs in flames. *Appl Phys B* 78:485–492
40. Hebert D, Coppalle A, Talbaut M (2013) 2d soot concentration and burning rate of a vertical pmma slab using laser-induced incandescence. *Proc Combust Inst* 34:2575–2582
41. Melton LA (1984) Soot diagnostics based on laser heating. *Appl Opt* 23:2201–2208
42. de Francqueville L, Bruneaux G, Thirouard B (2010) Soot volume fraction measurements in a gasoline direct injection engine by combined laser induced incandescence and laser extinction method. *SAE Int J Engines* 3:163–182
43. Widmann J, Yang JC, Smith T, Manzello S, Mulholland GW (2003) Measurement of the optical extinction coefficients of post-flame soot in the infrared. *Combust Flame* 134:119–129
44. Williams TC, Shaddix CR, Jensen KA, Suo-Anttila JM (2007) Measurement of the dimensionless extinction coefficient of soot within laminar diffusion flames. *Int J Heat Mass Transfer* 50:1616–1630
45. Zhao H, Ladommatos N (1998) Optical diagnostics for soot and temperature measurement in diesel engines. *Prog Energy Combust Sci* 24:221–255
46. Chen X, Lu S (2018) Fire-induced horizontal vent flow pattern in a ceiling vented enclosure: theoretical analysis and experimental verification. In: *Asia-Oceania symposium on fire science and technology*, pp 167–179
47. Beji T, Zhang J, Delichatsios M (2008) Soot formation and oxidation in fires from laminar smoke point measurements. *Fire Saf. Sci.* 9:219–230

Publisher's Note Springer Nature remains neutral with regard to jurisdictional claims in published maps and institutional affiliations.

Springer Nature or its licensor (e.g. a society or other partner) holds exclusive rights to this article under a publishing agreement with the author(s) or other rightsholder(s); author self-archiving of the accepted manuscript version of this article is solely governed by the terms of such publishing agreement and applicable law.